www.rericjournal.ait.ac.th

# An Optimised Hybrid Biomass Combined Cycle with Integrated Solar Thermal System

A.O. Ayeleso*,[1] and A.K. Raji*

**ARTICLE INFO**

*Article history:*
Received 04 November 2021
Received in revised form
17 March 2022
Accepted 08 April 2022

*Keywords:*
Biomass
Energy and exergy efficiencies
Gas turbine
Solar energy
Steam turbine

**ABSTRACT**

*In recent years, renewable sources of energy have become an encouraging solution to the environmental and availability problems arising from using fossil fuels for power generation. In the present study, solar and biomass (sawdust) are incorporated into large-scale gas and steam turbines to form a resourceful and efficient system. Furthermore, two hybrid configurations (fuel economy and energy boosting modes) of the proposed combined system are modelled using the Cycle Tempo software. The system's performances reveal that at 9 bar inlet pressure, the net power, energy and exergy efficiencies generated in the fuel economy mode (49 MWe, 61%, and 55%) and energy boosting mode (51 MWe, 64% and 57%) are significantly higher than those obtained in the standard biomass combined cycle system without solar fields (28 MWe, 35% and 31%). Moreover, the addition of solar energy brings about an increment of around 21 MWe in the fuel economy mode and 23 MWe in the energy boosting mode. The exergy transmitted from the fuel economy and energy boosting modes also yields greater GT combustor efficiency (89%) than the standard mode (79%). The proposed hybrid system through the incorporated clean energy offers better performance and could serve as an alternative to existing fossil fuel plants.*

## 1. INTRODUCTION

Over the past years, the generation of power through non-renewable energy resources such as fossil fuels have contributed immensely to increased environmental pollution [1], [2]. Aside from this, the major concern of the energy sector is the increasing levels of carbon dioxide ($CO_2$) emission in developing countries. Hence, there is a need to find alternative and efficient technologies for the conversion of existing conventional and untapped renewable resources. A promising approach is to combine renewable sources such as biomass and solar with conventional power plants in a hybrid system [3].

Biomass is available in several forms such as eucalyptus, twigs, bamboo, rice straw, wood chips, sawdust, animal waste and household waste [4]. The conversion of biomass to gaseous fuel can be done using either thermal, chemical, thermochemical and biochemical methods [3], [5].

The thermochemical method, also known as gasification, is a process in which biomass and moisture contents undergo partial combustion at high temperature to produce a syngas (producer gas) mixture [3], [6], [7]. The syngas is composed of elements such as carbon monoxide (CO), water ($H_2O$), carbon (IV) oxide ($CO_2$), hydrogen ($H_2$), nitrogen ($N_2$) and methane ($CH_4$). Furthermore, the syngas is often controlled by gasifying agents such as enriched air, steam and oxygen. A typical syngas has a low heating value (LHV) that ranged from 4 to 6 MJ/Nm$^3$ when air is used. Whereas when either steam or oxygen is used, the LHV ranged from 12 to 18 MJ/Nm$^3$ [8], [9]. The biomass syngas can also be used alongside a solar energy source and technology such as gas turbine (GT) to produce high electric power. This approach gives better performance and could reduce cost compared to the fossil engine systems [10], [11].

Solar energy is a clean and cost-effective type of renewable source [12]. This energy can be harnessed through technologies such as photovoltaics (PV), solar power tower (SPT), and heating systems.

The SPT is a concentrated solar power (CSP) system that can be used for the generation of heat and electricity [13]. The system consists of several heliostats, which concentrate sun radiation energy to a volumetric-type receiver (VTR) inside a fixed tower. In the VTR, fluid such as liquid and gases are heated to high temperatures and then injected to either GT or steam turbine (ST) for power generation [14]-[18]. The pressurised solar VTR can heat fluids to a temperature of about 800 °C at 10 bar [14], [19]-[25].

Several literatures have been conducted in the past to investigate the thermodynamic performance and cost predictions regarding the coupling of solar and biomass sources to combined cycle power plants [3], [26]-[37].

Camporeale *et al.* [30] conducted a study that investigated the technical and economic performance of

*Department of Electrical, Electronics and Computer Engineering, Cape Peninsula University of Technology (CPUT), P.O. Box 1906, Bellville 7535, Cape Town, South Africa.

[1]Corresponding author:
E-mail: ayelesoayokunle@gmail.com; ayelesoa@cput.ac.za

a mix system consisting of biomass gasifier, externally fired GT cycle and ORC units. It was reported that a higher electrical efficiency was achieved in the combined cycle system compared to a single cycle option (GT only). Moreover, the incorporation of the ORCs makes power generation more profitable. It is worth noting that a loss of efficiency was observed due to superheating in the ORC subcritical cycles. Hence, it was recommended that future cycles must be used with steam temperature values close to the critical point (saturation) regions.

In other research, Khanmohammadi *et al.* [38] conducted a study that investigated a combined cycle plant. The system comprises of a biomass gasifier, GT and ORC. The power output generated from this system was 1961.3 kWe, while the optimised exergy efficiency of the plant was 17.9 %. The estimated cost was 75 $/h.

Mondal and Ghosh [32] also investigated a combined cycle plant fuelled by a biomass gasifier unit. The output power obtained from this system was 914 kWe, while the energy efficiency of the plant was 41%. It was revealed that the electricity cost of the plant reduced to 0.069 $/kWh when the ratio of the compressor pressure, $r_c$, and inlet temperature of the turbine were set to 6 and 850 °C, respectively.

In another study, Mondal and Ghosh [33] performed a thermo-economic study on a 1-MW hybrid plant consisting of a biomass gasification system, an indirectly fired GT unit (inlet temperature of 1100 °C) and an organic Rankine cycle (ORC). The unit and production cost (UPC) of electricity from this system were 0.11 $/kWh and 5.3 $/GJ, respectively.

Morrone *et al.* [36] analysed several cogenerate ORC's for residential applications in southern Italy. The hybrid system was fuelled using in-series biomass boilers and parabolic-trough collectors (PTCs). The performance analysis results showed that the biomass consumption rates (about 21.0%) in the hybrid system was lower compared to heat engines that were fuelled by biomass only. Moreover, the combination of the heat sources within the system produces a higher net energy efficiency (67%) and increased maximum operating hours.

Chattopadhyay and Ghosh [3] performed a study that investigated the feasibility of integrating a biomass-based system (gasifier) to a cooling plant (combined cycle) in a remote village that has no access to the grid. The results showed that the plant capacity and daily operation time needed to meet the village electricity demand were 100 kWe and 10 hrs, respectively. The efficiency of the system was 23%.

In another study, Chattopadhyay and Ghosh [37] investigated a triple combined system that consists of a wood gasifier, a GT unit and an array of solar flat-plate collectors. The net energy efficiency of the combined system ranged from 59 to 76%, while the net exergy efficiency ranged from 19 to 26.5%. The efficiency of the GT (inlet temperature of 1100 °C) is 27.5 %.

Pantaleo *et al.* [35] investigated a hybrid system that consist of a wood chip gasifier, a GT, an ORC unit and PTCs running on molten salts fluid. A thermal-energy storage unit (TSU) was also placed between the GT, ORC, and PTCs to increase the solar input levels and to minimise the Cost of Electricity (COE). Their results revealed that about 1.3 MW was delivered by the GT system. Whereas in the ORC system, a power of 0.7 MW (with solar) and 0.8 MW (without solar) were achieved. The global efficiency of the system was 25%.

Liu *et al.* [39] performed another study on two hybrid cogeneration systems coupled to a biomass gasifier.

In the first system, a VTR was utilized in the gasification process to produce a syngas, which was then expanded in the Brayton cycle (BC). In the second system, the VTR was directly used in the BC to preheat the air exiting the GT compressor. This method helped to reduce the fuel consumption rate in the system. The exergy efficiency obtained from the first and second systems were 34.92% and 33.30%, respectively.

The aforementioned literature reviews have indicated that either a solar field or a biomass has been incorporated to a combined cycle system. Through a preliminary comparison, each method taking individually appeals with benefits such as energy loss reduction (during intermediate energy conversion process), generation of the required heat needed in the Rankine cycle (RC), increased net power and high efficiency.

Despite the knowledge gained from the previous studies, systems harnessing both solar fields and biomass energies simultaneously have not been thoroughly investigated. Reports are also sparse on the deep optimization of biomass combined cycle (BCC) and SPT systems to achieve optimum power and high efficiency. An attempt to reduce the gap through this study, has been to investigate a hybrid system that involves the combination of BCC and a solar field unit (*i.e.*, SBCC) using the Cycle-Tempo software. The biomass considered for the proposed system is a sawdust. This renewable energy source is selected mainly because it is clean, abundant in nature and its applications are enormous in regions where fossil fuel resources are either limited or restricted.

## 2. SYSTEM CONFIGURATION

The BCC and SBCC systems consist of a biomass unit, a gasifier unit, and a combined cycle (GT and ST) unit. The main distinction between these two systems is the addition of solar energy in the SBCC system. In this study, the optimisation of the SBCC system is performed using two different modes of operation: fuel economy mode (FEM) and energy boosting mode (EBM).

In the FEM, hot air from a VTR on top of an SPT unit is employed to preheat air exiting the GT compressor using a non-contact heat exchanger (NCHE 1) before reaching the combustor unit. Thereafter, the compressed hot air is mixed with biomass syngas inside the combustor, resulting to a high temperature flue gas. Subsequently, the flue gas is expanded in the turbine for power generation [17], [40]-[42].

In the EBM, the mode of operation is like that of the FEM. The difference between the two modes is that

in the EBM, the hot air from the solar VTR is also used in the NCHE 2 to reheat the flue gas exiting the GT exhaust, as shown in Figure 1. This approach helps to achieve optimum net power, high efficiencies, and the required steam for the ST cycle.

To carry out this modelling, the performance of the BCC system (standard mode, SM) is initially analysed and thereafter, the FEM and EBM are modelled. Their performances are then compared to that of the SM.

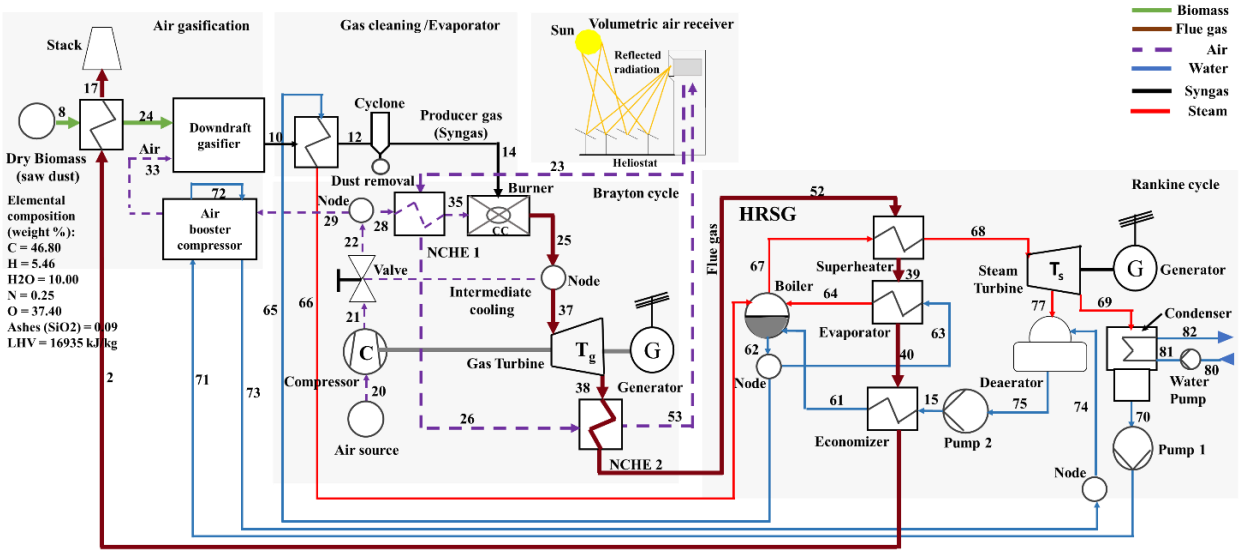


**Fig. 1. Schematic diagram showing the EBM structure of the SBCC system.**

## 3. THERMAL PRINCIPLES OF THE SBCC SYSTEM

### *3.1 Biomass Gasification System*

The biomass gasifier system modelled in the present study is primarily a downdraft type. Other subsystems include a gas cooling unit, and a cleaning unit to remove tar, ash, and dust contaminations. Table 1 presents the characteristics of the applied sawdust and the stationary bed gasifier. These parameters are similar to those found experimentally in the literature [43]-[45].

**Table 1. Biomass composition and gasifier characteristics.**

| Gasifier parameters | Present model | Fortunato Modelled Gasifier | Altafini Experimental Gasifier |
|---|---|---|---|
| Type | Stationary-bed Downdraft | Stationary-bed Downdraft | Stationary-bed Downdraft |
| Gasification agent | Air | Air | Air |
| Operating pressure (bar) | 25 | 1.013 | 0.93 |
| Preheated air temperature (°C) | 99 | 18 | 20 |
| Oxidant / biomass ratio | 1.67 | 2.07 | 1.83 |
| | | | |
| Fuel specifications | | | |
| Biomass | Saw dust | Saw dust | Saw dust |
| Maximum consumption (kg $h^{-1}$) | ≈ 12.6 | ≈ 12 | ≈ 12 |
| | | | |
| Element composition | | | |
| C (%) | 52.00 | 52.00 | 52.00 |
| H (%) | 6.07 | 6.07 | 6.07 |
| N (%) | 0.28 | 0.28 | 0.28 |
| O (%) | 41.55 | 41.55 | 41.55 |
| $S_iO_2$ (Ash) content (%) | 0.10 | 0.10 | 0.10 |
| Moisture ($H_2O$) content (%) | 10 | 10 | 11 |
| LHV (kJ/kg) | 16935 | 16935 | 19087 |
| | | | |
| Gasifier output | | | |
| Outlet temperature (°C) | 908.29 | 850 | 832 |
| Pressure (bar) | 25 | 1.013 | 0.92 |

The pressure and temperature applied in the gasifier are 25 bar and 800 °C, respectively. The oxidant/biomass ratio, $X_{OF}$, is 1.67. An air booster compressor system of about 99 °C is applied at the gasifier inlet to increase the gasification efficiency.

For the gasification process, all reactions and pyrolysis products are presumed to be in chemical equilibrium before leaving the gasifier. Moreover, these products burn and achieves equilibrium reactions, as given by [46], [47],

$$C + CO_2 \rightarrow 2CO \quad (1)$$

$$C + H_2O \rightarrow CO + H_2 \quad (2)$$

$$C + 2H_2 \rightarrow CH_4 \quad (3)$$

The coupling of Equations (1) and (2) produce the water gas shift reaction, as given by,

$$CO + H_2O \rightarrow CO_2 + H_2 \quad (4)$$

The global equation of a biomass gasification reaction is given by [46], [48].

$$CH_aO_bN_c + wH_2O + m(O_2 + 3.76N_2) \rightarrow n_1H_2 + n_2CO + n_3CO_2 + n_4H_2O + n_5CH_4 + n_6N_2 \quad (5)$$

where $CH_aO_bN_c$ denotes the generalized unified chemical formula for a dry biomass fuel and m represents the ratio of the kilomoles of air against the kilomoles of biomass. The subscripts a, b, and c, denote paper and wood chemical formulas for a single carbon atom, and their values are $CH_{1.60}O_{0.765}N_{0.00592}$ and $CH_{1.44}O_{0.66}$, respectively [46], [49]. The coefficients $n_1$ to $n_6$ represent the number of each gas specie in moles ($H_2$, $CO$, $CO_2$, $H_2O$, $CH_4$ and $N_2$), while $w$ denotes the biomass moisture content, as given by [46],

$$w = \frac{M_{biomass}M_C}{18(1 - M_C)} \quad (6)$$

where $M_C$ represents the mass-based moisture content per moles of wood.

After the gasification process, the bio-syngas is separated from ash and then subsequently cleaned through a cyclone at 500 °C to remove dust, hydrogen sulphide ($H_2S$), tar and other sulphuric compounds. The gas cleaning process eliminates the contaminants without affecting the composition of the syngas. The expression used to determine the efficiency of the biomass gasifier is given as [37],

$$\eta_{gasification} = \frac{m_{p,gas} \cdot LHV_{p,gas}}{m_{biomass} \cdot LHV_{biomass}} \quad (7)$$

where $m_{p,gas}$ ($m_{14}$) represents the producer gas mass, $m_{biomass}$ ($m_8$) is the rate of biomass consumption, $LHV_{p,gas}$ represents the low heating value of syngas and $LHV_{biomass}$ denotes the biomass low heating value.

### 3.2 Gas Turbine Cycle

- *System description*

The gas turbine system modelled in this study applies the Brayton cycle principles. In this system, a GT compressor is first employed to preheat ambient air. Subsequently, the heat exchanger (NCHE 1) is incorporated between the compressor and combustor to further raise the fluid temperature. This approach often ensures that the fuel consumption rate is reduced, while increasing the flue gas temperature (Figure 1). The schematic diagram of temperature, *T*, versus entropy, *s*, in the GT system is depicted in Figure 2.

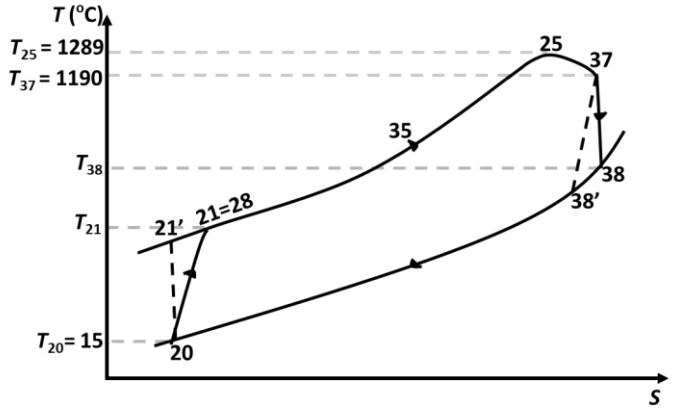


**Fig. 2. Temperature versus entropy in the GT system.**

The key processes in the GT system are given as follows [50]:

i. The isentropic compression is performed in the compressor from point 20 to 21.
ii. The preheated compressed air is performed from point 21 to 35.
iii. The addition of heat into the combustion chamber (CC) is performed from point 35 to 25.
iv. The intermediate cooling of the flue gas is performed from point 25 to 37.
v. The isentropic expansion is performed in the turbine from point 37 to 38.
vi. The heat rejection is performed from point 38 to 20.

The compressor exit temperature, $T_{21}$, (point 20 to 21) is given by [50],

$$T_{21} = T_{20} \cdot \left(1 + \frac{r_c^{\frac{\gamma_a - 1}{\gamma_a}} - 1}{\eta_c}\right) \quad (8)$$

where $\eta_c = T_{21}' - T_{20}/T_{21} - T_{20}$ represents the isentropic efficiency for the compressor, $T_{20}$ and $T_{21}$ denote the inlet and outlet temperatures for the compressor, $T_{21}'$ signifies the isentropic temperature at the compressor outlet and $\gamma_a$ = 1.4 denotes the air heat capacity ratio.

The adiabatic temperature of the turbine, $T_{38}'$, and the discharge temperature of the turbine, $T_{38}$, is given by [50], [51],

$$T_{38}' = \frac{T_{37}}{r_c^{\frac{\gamma_g - 1}{\gamma_g}}} \quad (9)$$

$$T_{38} = T_{37} - \eta_T \cdot (T_{37} - T_{38}') \quad (10)$$

where $T_{37}$ represents the temperature of combustion flue gas, $\gamma_g$ = 1.33 signifies the flue gas heat capacity ratio and $\eta_T$ denotes the turbine isentropic efficiency.

The NCHE 1 temperature (point 28 to 35) is given by,

$$T_{35} = T_{28} + \eta_{NCHE}(T_{38} - T_{28}) \quad (11)$$

The heat, $Q_{in}$, supplied after isentropic expansion in the turbine (point 37 to 38) is given by [52], [53],

$$Q_{in} = m_a \cdot cp_a \cdot (T_{37} - T_{28}) \quad (12)$$

where $m_a$ represents the mass rate for air, $cp_a$ = 1.0 $\mathrm{kJ/(kgK)}$ denotes the specific heat for air and $\eta_{NCHE}$ signifies the NCHE efficiency.

The work performed in the compressor, $W_C$, (point 20 to 21) is given by,

$$W_C = cp_a \cdot (T_{21} - T_{20}) \quad (13)$$

The work performed in the gas turbine, $W_{GT}$, (point 37 to 38) is given by [52], [53],

$$W_{GT} = cp_g \cdot (T_{37} - T_{38}) \quad (14)$$

where $cp_g$ = 1.15 $\mathrm{kJ/(kgK)}$ denotes the specific heat for flue gas.

The ratio of work in the turbine, $W_{ratio}$, is given as,

$$\mathrm{l}W_{ratio} = \frac{W_{GT} - W_C}{W_{GT}} \quad (15)$$

The amount of work performed in the GT, $W_{net\_GT}$, is given by [53],

$$W_{net\_GT} = (W_{GT} - W_C) \quad (16)$$

The total work or power in the Brayton cycle is given by,

$$W_{net\_GT} = \eta_{Bc} \times Q_{in} \quad (17)$$

The Brayton cycle thermal efficiency, $\eta_{Bc}$, is given by,

$$\eta_{Bc} = 1 - \frac{1}{(r_T)^{\frac{\gamma_g - 1}{\gamma_g}}} = \frac{(T_{37} - T_{38}') - (T_{21}' - T_{20})}{(T_{37} - T_{21}')} \quad (18)$$

### *3.3 Steam Turbine Cycle*

- *System description*

The steam turbine system modelled in this study applies the Rankine cycle principles. This system uses a heat recuperation steam generator (HRSG) to produce a hot steam. An advantage of using this approach is that it significantly help in the reduction of $CO_2$ emission from the GT exhaust. The HRSG unit is made up of a superheater, an evaporator and an economiser (Figure 1). The schematic diagram of temperature versus entropy in the ST system is depicted in Figure 3 [54].

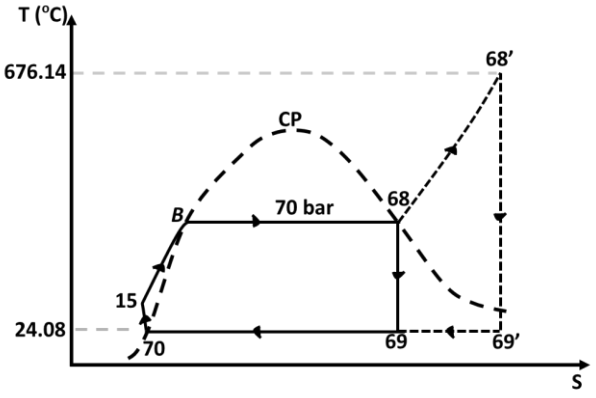


**Fig. 3. Temperature versus entropy in the ST system. Line 68-69-70-15-B-68 = saturated cycle. Line 68'-69'-70-15-B-68' = superheated cycle. CP = critical point.**

The key processes in the ST system are given as follows [55]:

i. The adiabatic reversible compression is performed in the condenser (point 70 to 15). In this process, the saturated liquid flowing from the condenser (point 70) is pumped to subcooled liquid at the HRSG (point 15).

ii. Process 15 to 68 or 15 to 68' is the constant-pressure heat addition in the steam generator. Line 15-*B*-68-68' is a constant-pressure line and *B* represents a boiler. Line 15-*B* in the Rankine cycle is called an economizer. It represents bringing the subcooled liquid at point 15 to the saturated liquid at point *B*. Line

*B*-68 in the cycle is the process involving the boiler and evaporator under a constant pressure of 70 bar. The process also signifies the heating of the saturated liquid to saturated vapor. Thereafter, the saturated vapor in the evaporator flows back to the boiler. Line 68-68' in the cycle is called a superheater. It represents heating the saturated vapor at point 68 to point 68'.

iii. Process 68-69 or 68'-69' is the adiabatic reversible expansion through the turbine. In this process, the high temperature steam flows through the rotating ST blades to produce electric power. The exhaust vapor at point 69 or point 69' is normally in the two-phase region stage.

iv. Process 69-70 is a two-phase mixture condensing stage, where heat rejection takes place in the condenser at constant pressure and temperature. The rejected vapor from the ST is then converted back to a liquid form and reused in the subsequent cycles.

The heat energy, $Q_{RC}$, supplied to the Rankine cycle is given by [55]-[57],

$$Q_{RC} = m_{RC}(h_{68} - h_{15}) \quad (19)$$

The work performed in the turbine, $W_{ST}$, is given by,

$$W_{ST} = m_{RC} \cdot (h_{68} - h_{69}) \quad (20)$$

The rejected heat , $q_r$, after the condenser stage is given by,

$$q_r = m_{RC} \cdot (h_{69} - h_{70}) \quad (21)$$

The work performed by the pump, $W_P$, is given by,

$$W_P = m_{RC} \cdot (h_{15} - h_{70}) \quad (22)$$

The total work, $W_{net\_ST}$, in the cycle is given by,

$$W_{net\_ST} = W_{ST} - W_P \quad (23)$$

$$W_{net\_ST} = m_{RC} \cdot [(h_{68} - h_{69}) - (h_{15} - h_{70})]$$

where $m_{RC}$ is the mass rate in the cycle, $h_{70}$ represents the pump enthalpy, $h_{15}$ is the preheater enthalpy, $h_{68}$ signifies the turbine enthalpy, and $h_{69}$ denotes the condenser enthalpy.

The Rankine cycle thermal efficiency, $\eta_{Rc}$ , is given by [55]-[57],

$$\eta_{RC} = \frac{W_{net\_ST}}{Q_{RC}} = \frac{(h_{68} - h_{69}) - (h_{15} - h_{70})}{h_{68} - h_{15}} \quad (24)$$

For the combined cycle (GT and ST), the net power and efficiency are given by [58],

$$W_{CC}{}^{net} = W_{GT} + W_{ST} - W_{AUX} \quad (25)$$

$$\eta_{CC}{}^{net} = \frac{W_{GT} + W_{ST}}{Q_{GT} + Q_{ST}} \times 100 \quad (26)$$

where $W_{GT}$ represents the work performed in the gas turbine, $W_{ST}$ signifies the work performed in the steam turbine, $W_{AUX}$ denotes the work consumed in the auxiliary, $Q_{GT}$ represents the heat delivered to the Brayton cycle and $Q_{ST}$ denotes heat delivered to the Rankine cycle.

## 4. RESULTS AND DISCUSSION

The performance analyses of the SBCC system under the SM, FEM and EBM at nominal design points are presented in this section.

### *4.1 Validation of the Stationary-bed Biomass Gasifier*

The production of biomass syngas through an air gasification technique is a vital part of the SBCC system. In this system, the syngas obtained from the downdraft gasifier is composed of sawdust, air and water (moisture content). Table 2 presents the results of the sawdust syngas (producer gas) produced in the current and past studies [43], [44].

The results presented in Table 2 show that the producer gas quality in the current model compared well with the syngas results found in previous studies [43], [44]. The $H_2$ and $CH_4$ contents are higher in the current model, while the CO, $N_2$, and $CO_2$ contents are lower compared to those obtained by Altafini *et al.* [43]. The LHV of the sawdust syngas is 4.61 (MJ/kg), while the high heating value (HHV) is 5.0 (MJ/kg). The efficiency of the gasifier is 85%.

**Table 2. Sawdust gasifier performance results: Present and previous models.**

| | Present Model Gasifier | Fortunato Gasifier | Altafini Experimental Gasifier |
|---|---|---|---|
| Sawdust syngas composition | | | |
| $H_2$ (%) | 15.95 | 14.95 | 14 |
| $CH_4$ (%) | 2.92 | 2.60 | 2.31 |
| CO (%) | 17.98 | 19.45 | 20.14 |
| $N_2$ (%) | 41.92 | 50.23 | 50.79 |
| $CO_2$ (%) | 11.41 | 12.16 | 12.06 |
| | | | |
| Gasifier output | | | |
| Outlet temperature (°C) | 908.29 | 850 | 832 |
| Pressure (bar) | 25 | 1.013 | 0.92 |
| Gasification efficiency (%) | 85 | 73 | 63 |

**Table 3. The performance results of the SBCC system under SM, FEM, and EBM at 9 bar.**

Standard mode (without solar fields)

| Descriptions | No | Equipment | Type | Energy | Totals | Exergy | Totals |
|---|---|---|---|---|---|---|---|
| Consumed power (kW) | 16 | Source & Sink | 10 | 79594.50 | 79594.50 | 89130.62 | 89130.62 |
| | 1 | GT Generator | GT_G | 18063.40 | | 18063.40 | |
| | 2 | ST Generator | ST_G | 11282.73 | | 11282.73 | |
| Gross power (kW) | | | | | 29346.13 | | 29346.13 |
| Power consumed by auxiliaries (kW) | 29 | Compressor | 29 | 1230.63 | | 1230.63 | |
| | 48 | Pump-one | 8 | 9.29 | | 9.29 | |
| | 53 | Pump-two | 8 | 135.96 | | 135.96 | |
| | 61 | Pump-three | 8 | 129.72 | | 129.72 | |
| | | | | | 1505.61 | | 1505.61 |
| Net power (kW) | | | | | 27840.53 | | 27840.53 |
| Efficiencies | gross | | | 36.870 % | | 32.925 % | |
| | net | | | 34.978 % | | 31.236 % | |

FEM

| Descriptions | No | Equipment | Type | Energy | Totals | Exergy | Totals |
|---|---|---|---|---|---|---|---|
| Consumed power (kW) | 16 | Source & Sink | 10 | 79594.50 | 79594.50 | 89130.62 | 89130.62 |
| | 1 | GT Generator | GT_G | 30144.23 | | 30144.23 | |
| | 2 | ST Generator | ST_G | 20073.46 | | 20073.46 | |
| Gross power (kW) | | | | | 50217.70 | | 50217.70 |
| Power consumed by auxiliaries (kW) | 29 | Compressor | 29 | 1230.63 | | 1230.63 | |
| | 14 | Pump-one | 8 | 0.00 | | 0.00 | |
| | 48 | Pump-two | 8 | 12.53 | | 12.53 | |
| | 53 | Pump-three | 8 | 194.33 | | 194.33 | |
| | 61 | Pump-four | 8 | 203.59 | | 203.59 | |
| | | | | | 1641.09 | | 1641.09 |
| Net power (kW) | | | | | 48576.61 | | 48576.61 |
| Efficiencies | gross | | | 63.092 % | | 56.342 % | |
| | net | | | 61.030 % | | 54.500 % | |

EBM

| Descriptions | No | Equipment | Type | Energy | Totals | Exergy | Totals |
|---|---|---|---|---|---|---|---|
| Consumed power (kW) | 16 | Source & Sink | 10 | 79594.50 | 79594.50 | 89130.62 | 89130.62 |
| | 1 | GT Generator | GT_G | 30144.23 | | 30144.23 | |
| | 2 | ST Generator | ST_G | 22349.00 | | 22349.00 | |
| Gross power (kW) | | | | | 52493.23 | | 52493.23 |
| Power consumed by auxiliaries (kW) | 29 | Compressor | 29 | 1230.63 | | 1230.63 | |
| | 14 | Pump-one | 8 | 0.00 | | 0.00 | |
| | 48 | Pump-two | 8 | 13.26 | | 13.26 | |
| | 53 | Pump-three | 8 | 206.08 | | 206.08 | |
| | 61 | Pump-four | 8 | 220.48 | | 220.48 | |
| | | | | | 1670.45 | | 1670.45 |
| Net power (kW) | | | | | 50822.78 | | 50822.78 |
| Efficiencies | gross | | | 65.951 % | | 58.895 % | |
| | net | | | 63.852 % | | 57.021 % | |

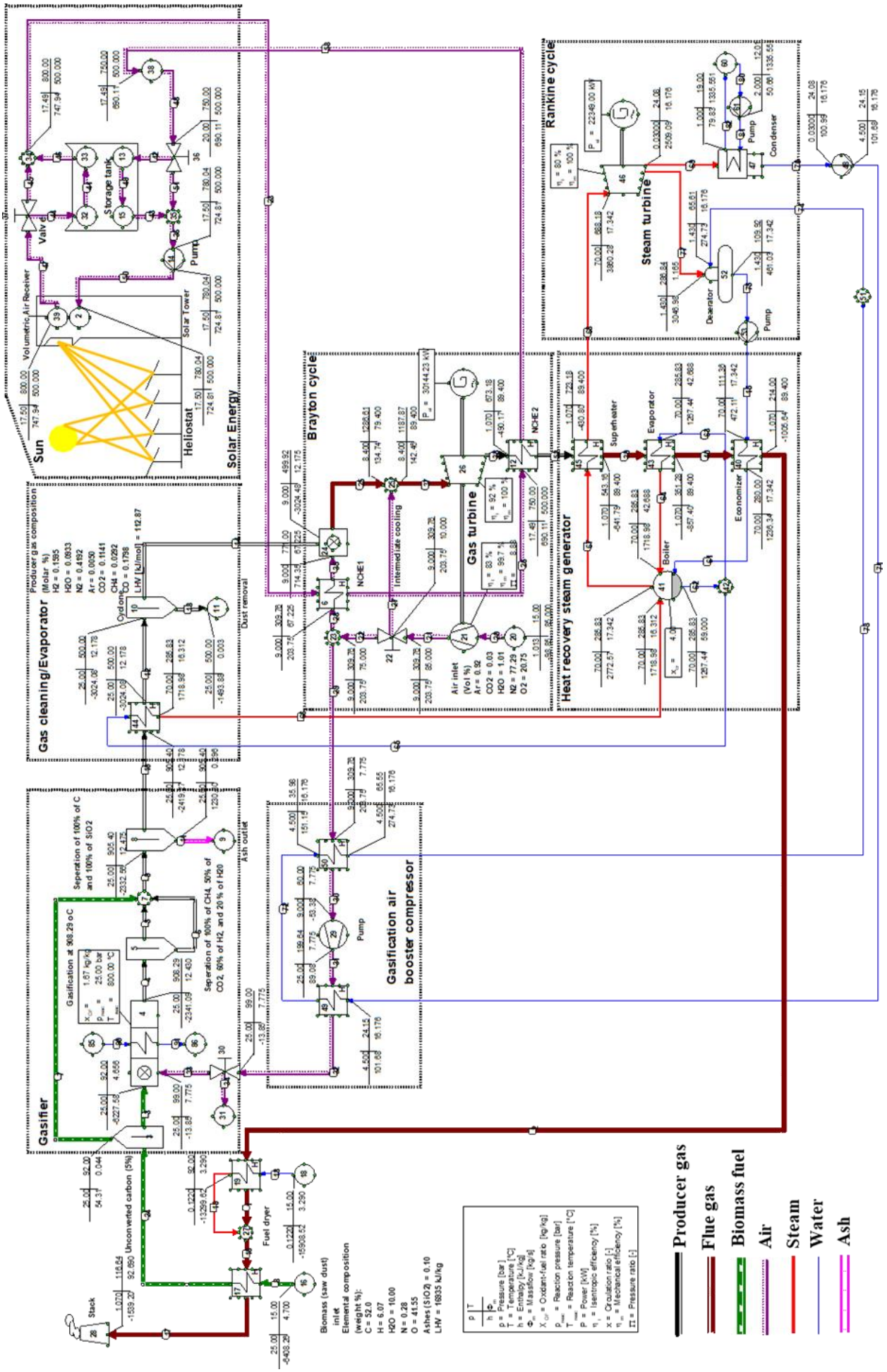


**Fig. 4. The flow process of the SBCC system under the EBM at 9 bar.**

### *4.2 The SBCC System Modelling Results*

The hybrid SBCC system considered in this study is composed of a biomass gasifier, a solar field, an ST, and a GT (Figure 1). In this system, two different modes (FEM and EBM) are modelled and compared to a BCC (SM) system with no solar fields. To configure the SBCC system, a solar VTR data, with an outlet temperature of 800 °C [59]-[60] is introduced directly into the system through the heat exchangers (NCHE 1 and NCHE 2) in the Cycle Tempo software (Figure 4).

The inlet temperature and constant compressor pressure of the SBCC GT in the FEM and EBM are 1187.87 °C and 9 bar, respectively. Whereas in the SM, the GT inlet temperature is 879.92 °C at a pressure of 9 bar. Table 3 presents the performance results of all the modes (SM, FEM and EBM). Figure 4 presents the flow process of the SBCC system under the EBM.

From the thermodynamics standpoint, the EBM (energy = 64% and exergy = 57%) produces a higher efficiency compared to the FEM (energy = 61% and exergy = 55%) and SM (energy = 35% and exergy = 31%). Similarly, the net efficiency delivered in the FEM and EBM is greater than those obtained in the SM. Moreover, the efficiency obtained under the FEM and EBM is significantly higher than those (energy = 30.88% and exergy = 33.30%) found in Liu *et al.* [39], which uses a GT turbine inlet temperature of 1287.85 °C.

The net power delivered under the EBM is approximately 51 MWe (30.1 MWe GT power, 22.4 MWe ST power and 1.7 MWe auxiliary power), as shown in Table 3. Whereas the net power delivered in the FEM and SM is 49 MWe (30.1 MWe GT power, 20.1 MWe ST power and 1.6 MWe auxiliary power) and 28 MWe (18.1 MWe GT power, 11.3 MWe ST power and 1.51 MWe auxiliary power), respectively. The above results show that the net power produced in the EBM and FEM is higher than those obtained in the SM. Comparing these results to previous studies, the power generated under the EBM (51 MWe) and FEM (49 MWe) compares well with the 49.3 MWe found in Liu *et al.* [39].

Referring to Table 3, the elevated power delivered by the ST under the EBM and FEM is due to the incorporated solar energy and GT exhaust flue gas. In the EBM, an inlet temperature of 688.18 °C is obtained in the ST using a GT flue gas of 723.18 °C. Whereas in the FEM and SM, the ST inlet temperatures of 638.18 °C and 425.21 °C are obtained using the GT flue gas of 673.18 °C and 460.21 °C, respectively.

The variation of the GT compressor pressure between 5 bar and 15 bar contributes significantly to the overall power generated from the different modes. When the pressure is increased from 9 to 15 bar, the power output decreases from 28 to 25 MWe in the SM. Similarly, the power output decreases from 49 to 46 MWe in the FEM and from 51 to 48.4 MWe in the EBM (Figure 5). When the pressure is decreased from 9 to 5 bar, the power output decreases from 28 to 26 MWe (SM), from 49 to 45 MWe (FEM) and from 51 to 47 MWe (EBM), as shown in Figure 5.

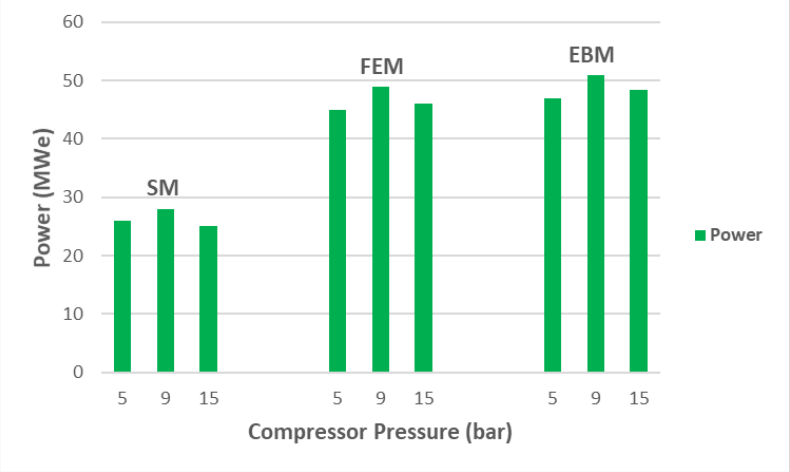


**Fig. 5. Power generated under varying pressures in the SM, FEM, and EBM.**

To make a broad comparison of the power generated from each mode (Figure 5), an observation worth noting is that irrespective of the applied pressure, the hybrid SBCC (EBM and FEM) systems still produce the best power performance compared to the BCC (SM) system. This shows that a better solar share is utilised in the EBM and FEM, which implies a lower COE. The results also show that for a given biomass composition and GT inlet temperature, the net power delivered at 9 bar is higher in all the modes compared to when 5 bar and 15 bar are applied.

The variation of the compressor pressure (5 to 15 bar) also contributes to the exergy transmitted from the combustor, GT and ST units (Figure 6).

The exergy transmitted from the combustor under the FEM and EBM (5 bar: 12144.82 kW, 9 bar: 11399.01 kW, 15 bar: 10775.2 kW) is lesser than that of the SM (5 bar: 18694.1 kW, 9 bar: 16689.66 kW, 15 bar: 15134.74 kW), as shown in Figure 6a. The exergy transmitted from the combustor unit is higher due to elevated temperature variation at the inlet and outlet of the system [38]. Furthermore, the exergy transmitted

under the FEM and EBM yields greater combustor efficiencies (89%) compared to the SM (79%). This is due to the minimal exergy destruction that occurs in both modes.

The exergy transmitted from the GT under the FEM and EBM (5 bar: 1082.86 kW, 9 bar: 1535.71 kW, 15 bar: 1532.6 kW) is lesser than that of the SM (5 bar: 1091.68 kW, 9 bar: 1552.09 kW, 15 bar: 1547.73 kW), as shown in Figure 6b.

The exergy transmitted from the ST under the FEM (5 bar: 5566.55 kW, 9 bar: 4964.41 kW, 15 bar: 5556.22 kW) and EBM (5 bar: 6143.85 kW, 9 bar: 5527.17 kW, 15 bar: 6134.16 kW) is higher than that of the SM (5 bar: 3127.72 kW, 9 bar: 2790.35 kW, 15 bar: 3268.58 kW), as shown in Figure 6c.

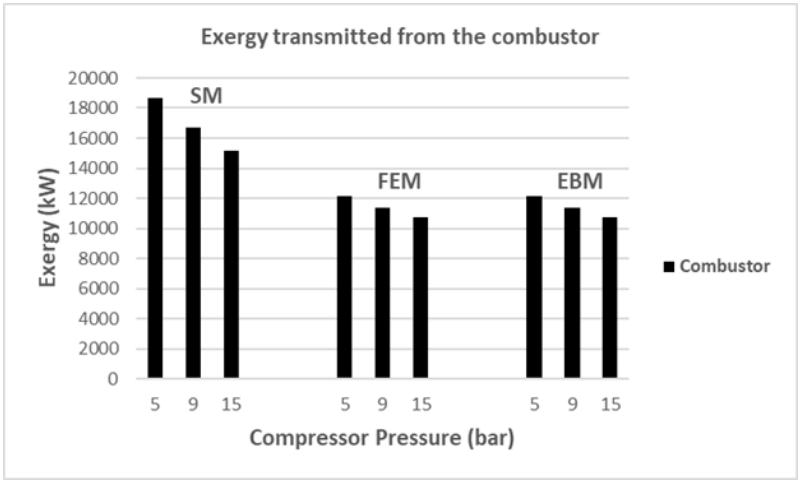


(a)

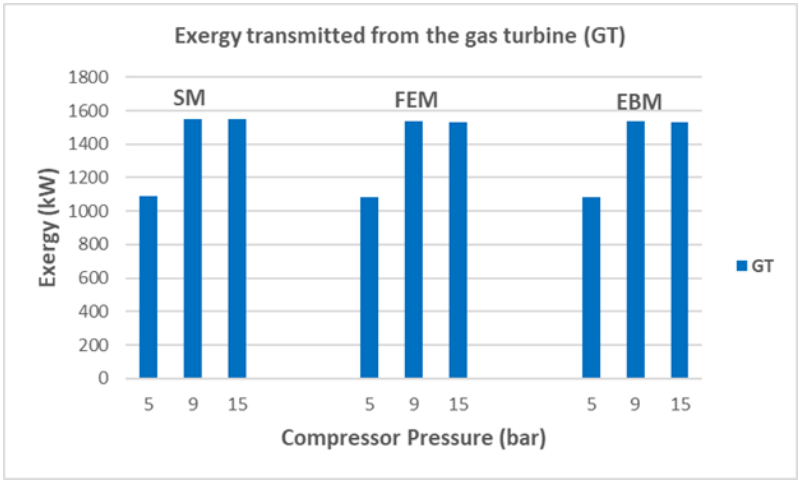


(b)

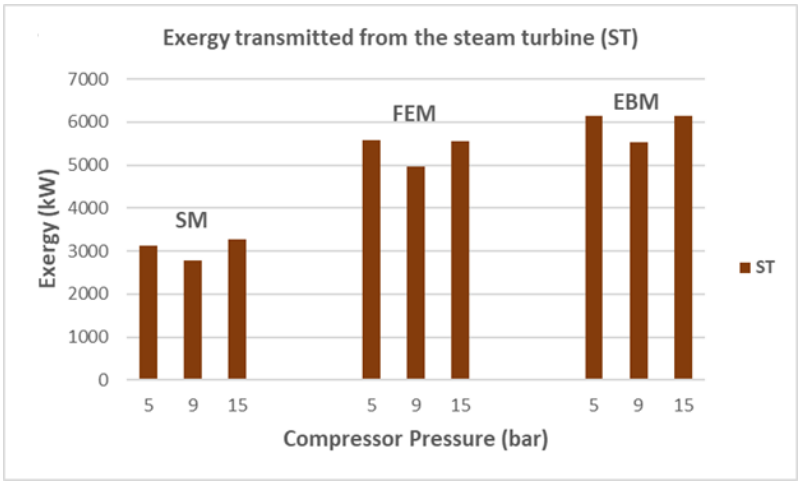


(c)

**Fig. 6. Exergy transmitted under varying pressures in SM, FEM, and EBM from: (a) The combustor unit, (b) The GT unit, (c) The ST unit.**

The exergy analyses in Figure 6a and 6b show that the combustor and GT units produce the best performance under the EBM and FEM unlike in the SM. Moreover, the incorporation of biomass (sawdust) and solar energy in the SBCC system could contribute to significant cost reduction unlike the conventional systems [59]-[62]. The use of clean energy in the conventional plants helps to reduce the rate of consumption of fossil fuels and natural gases. This approach also helps to minimize environmental pollution such as high turbine exhaust fumes and $CO_2$ emissions.

In future studies, more investigations would be conducted to evaluate the performance of the optimised SBCC system using sawdust and cow dung mixtures. The outcomes could intensify the sustainability of biomass for rural electrification, decrease the cutting down of trees, and reduce the harmful effect of manure decomposition in the environment.

## 5. CONCLUSION

An optimised hybrid SBCC system consisting of a solar field, a biomass gasifier, an ST, and a GT have been modelled in this study for large power generation. For the SBCC system optimisation routine, two different modes of operation (FEM and EBM) are investigated under nominal conditions from the viewpoints of power, efficiencies, and environmental terms. The performance of the SBCC system under the FEM and EBM are compared to the BCC (SM) system. This yielded insights into the system's operation. The major findings are summarised below:

- The sawdust gasification produces a cold gas efficiency of 85%, with LHV of 4.61 MJ/kg and HHV of 5.0 MJ/kg.
- The energy and exergy efficiencies in the SBCC system under the EBM and FEM are higher than those obtained in the SM.
- The net power generated in the SBCC system under the FEM and EBM is higher compared to the SM. Moreover, the high output power achieved in the EBM signifies a better and suitable system.
- The optimum exergy level is obtained in the combustor. Moreover, the exergy efficiency realised in the combustor at a pressure of 9 bar is higher in both FEM and EBM (89%) than in the SM (79%).
- The net power delivered at a 9 bar compressor pressure is higher in all the modes compared to when 5 bar and 15 bar are applied.
- The exergy transmitted from the combustor when the compressor pressure is varied between 5 bar and 15 bar is lesser in the FEM and EBM than in the SM. Likewise, the exergy transmitted from the GT when the pressure is varied between 5 bar and 15 bar decreases in the FEM and EBM as compared to the other mode. Conversely, in the ST, higher exergy losses are recorded in the FEM and EBM.

The above findings revealed the performance (benefits and limitations) that should be taken into consideration when designing an optimised SBCC system. The system could offer enormous opportunities to utilise the existing, reliable and sustainable energy. It could also serve as an alternative to the conventional power plants, especially in regions where fossil fuel resources are either limited or restricted.

## ACKNOWLEDGEMENT

The authors recognize the Cape Peninsula University of Technology for the financial support to this work. Appreciation also goes to Asimptote company for providing the Cycle Tempo software.

## NOMENCLATURE

***Symbols***

| | |
|---|---|
| $CH_aO_bN_c$ | Generalized formula for biomass fuel [dimensionless] |
| m | Kilomoles of air per kilomoles of biomass [kmol/kmol] |
| $n_1$ - $n_6$ | Number of moles [mol] |
| $w_1$ | Moisture content of biomass [%] |
| $M_C$ | Mass based moisture content per mole of wood [kg] |
| w | Moisture content of biomass [%] |
| $m_{p,gas}$ | Mass of producer gas [kg] |
| $m_{biomass}$ | Biomass consumption rate [kg $h^{-1}$] |
| $LHV_{p,gas}$ | Low heating value for syngas [MJ/kg] |
| $LHV_{biomass}$ | Low heating value for biomass [MJ/kg] |
| $\eta_c$ | Isentropic efficiency of the compressor [%] |
| $T_{20}$ | Inlet temperatures of the compressor [°C] |
| $T_{21}$ | Exit temperatures of the compressor [°C] |
| $T_{21}{}'$ | Isentropic temperature at the compressor outlet [°C] |
| $r_c$ | Pressure ratio of the compressor [dimensionless] |
| $\gamma_a$ | Air heat capacity ratio [dimensionless] |
| $T_{38}{}'$ | Adiabatic temperature of the turbine [°C] |
| $T_{38}$ | Discharge temperature of the turbine [°C] |
| $T_{37}$ | Temperature of combustion flue gas [°C] |
| $\gamma_g$ | Flue gas heat capacity ratio [dimensionless] |
| $\eta_T$ | Turbine isentropic efficiency [%] |
| $T_{35}$ | Temperature of heat exchanger [°C] |
| $\eta_{NCHE}$ | Efficiency of the heat exchanger [%] |
| $Q_{in}$ | Heat supplied to gas turbine [Joule/sec.] |
| $m_a$ | Mass of the air medium [kg/s] |

| | |
|---|---|
| $cp_a$ | Specify heat for air [k J/(k$_g$K)] |
| $W_C$ | Work performed by compressor [k J/(k$_g$K)] |
| $W_{GT}$ | Work performed by the GT [k J/(k$_g$K)] |
| $cp_g$ | Flue gas specific heat [k J/(k$_g$K)] |
| $r_T$ | Ratio of pressure in the turbine [dimensionless] |
| $W_{ratio}$ | Ratio of the work done [dimensionless] |
| $W_{net\_GT}$ | Net power delivered by the gas turbine [kW] |
| $\eta_{Br}$ | Brayton cycle efficiency [%] |
| $Q_{RC}$ | Heat energy flow input to RC [kW] |
| $W_{ST}$ | Work performed by the steam turbine [kW] |
| $W_P$ | Work performed by the pump [kW] |
| $W_{net\_ST}$ | Net power delivered by the steam turbine [kW] |
| $q_r$ | Rejected heat after the condenser stage [kW] |
| $\eta_{RC}$ | Thermal efficiency of RC [%] |
| $m_{RC}$ | Rankine cycle mass rate [kg/s] |
| $h_{70}$ | Enthalpy in the pump [kJ/kg] |
| $h_{69}$ | Enthalpy in the condenser [kJ/kg] |
| $h_{15}$ | Preheaters enthalpy [kJ/kg] |
| $h_{68}$ | Turbine enthalpy [kJ/kg] |
| $WAUX$ | Consumed work by the auxiliary [kW] |
| ${W_{CC}}^{net}$ | Net power of gas and steam turbines [kW] |
| ${\eta_{CC}}^{net}$ | Net efficiency of gas and steam turbines [%] |
| $Q_{GT}$ | Heat delivered to the Brayton cycle [kW] |
| $Q_{ST}$ | Heat delivered to the Rankine cycle [kW] |

***Abbreviations***

| | |
|---|---|
| LHV | Low heating value |
| GT | Gas turbine |
| PV | Photovoltaics |
| CSP | Concentrated solar power |
| SPT | Solar power tower |
| VTR | Volumetric-type receiver |
| ST | Steam turbine |
| BCC | Biomass combined cycle |
| RC | Rankine cycle |
| UPC | Unit product cost |
| PTCs | Parabolic-trough collectors |
| COE | Cost of electricity |
| BC | Brayton cycle |
| HRSG | Heat recuperation steam generator |
| TSU | Thermal-energy storage unit |
| RC | Rankine cycle |
| SBCC | Solar-biomass combined cycle |
| FEM | Fuel economy mode |
| EBM | Energy boosting mode |
| NCHE | Non-contact heat exchanger |
| FB | Fixed-bed |
| $X_{OF}$ | Oxidant to biomass ratio |
| $H_2S$ | Hydrogen sulphide |
| $T$ | Temperature |
| $s$ | Entropy |
| MW | Megawatt |
| CC | Combustion chamber |
| HHV | High heating value |

## REFERENCES


[1] Gorjian S., Zadeh B.N., Eltrop L., Shamshiri R.R. and Amanlou Y., 2019. Solar photovoltaic power generation in Iran: Development, policies, and barriers. *Renewable and Sustainable Energy Reviews* 106: 110-123. DOI: https://doi.org/10.1016/j.rser.2019.02.025

[2] Quaschning V.V., 2019. *Renewable Energy and Climate Change*. 2nd ed. USA: John Wiley & Sons. DOI: 10.1002/9781119514909

[3] Chattopadhyay S. and S. Ghosh. 2018. Feasibility study of a biomass gasification based combined power and cooling plant for an off-grid village. In *IOP Conference Series: Materials Science and Engineering, volume 377, International Conference on Mechanical, Materials and Renewable Energy*. Sikkim, India, 8–10 December 2017. Bristol: IOP Publishing Ltd. DOI: https://doi.org/10.1088/1757-899X/377/1/012003

[4] Lauri P., Havlik P., Kindermann G.E., Forsell N., Bottcher H., and Obersteiner M., 2014. Woody biomass energy potential in 2050. *Energy Policy* 66: 19-31. DOI: https://doi.org/10.1016/j.enpol.2013.11.033

[5] Barman N.S., Ghosh S., and De S., 2012. Gasification of biomass in a fixed-bed downdraft gasifier-A realistic model including tar. *Bioresource Technology* 107: 505-511. DOI: 10.1016/j.biortech.2011.12.124

[6] Zainal Z.A., Ali R., Lean C.H., and Seetharamu K.N., 2001. Prediction of performance of a downdraft gasifier using equilibrium modelling for different biomass materials. *Energy Conversion and Management* 42: 1499–1515. DOI: https://doi.org/10.1016/S0196-8904(00)00078-9

[7] Srinivas T., Reddy B.V., and Gupta A.V.S.S.K.S., 2009. Thermodynamic equilibrium model and exergy analysis of a biomass gasifier. *Journal of Energy Resources Technology* 131: 031801. DOI: https://doi.org/10.1115/1.3185354

[8] Mendiburu A.Z., Carvalho J.A., and Coronado C.J.R., 2014. Thermochemical equilibrium modelling of biomass downdraft gasifier: stoichiometric models. *Energy* 66: 189–201. DOI: https://doi.org/10.1016/j.energy.2013.11.022

[9] Puig-Arnavat M., Bruno J.C., and Coronas A., 2014. Modelling of trigeneration configurations based on biomass gasification and comparison of performance. *Applied Energy* 114: 845–856. DOI: 10.1016/j.apenergy.2013.09.013

[10] Paisley M.A. and M.J. Welch. 2003. Biomass gasification combined cycle opportunities using the future energy SilvaGas® gasifier coupled to Alstom's industrial gas turbines. *American Society of Mechanical Engineers (ASME) Turbo Expo* 1: 211–217. DOI: https://doi.org/10.1115/GT2003-38294

[11] Ghosh S., 2017. Biomass-based distributed energy systems: opportunities and challenges. In A. Gautam, S. De, A. Dhar, J.G. Gupta, and A. Pandey, 1st ed. *Sustainable Energy and Transportation: Energy, Environment, and Sustainability*. Singapore: Springer, pp. 235–252. DOI: https://doi.org/10.1007/978-981-10-7509-4_13

[12] Sukhatme S.P. and J.K. Nayak. 2008. *Solar Energy: Principles of Thermal Collection and Storage*; 3rd ed; India: Tata Mc-Graw Hill Publication.

[13] Požívil P., Aga V., Zagorskiy A., and Steinfeld A., 2014. A pressurized air receiver for solar-driven gas turbines. *Energy Procedia* 49: 498–503. DOI: https://doi.org/10.1016/j.egypro.2014.03.053.

[14] Kalogirou S.A., 2011. Concentrating solar power plants for electricity and desalinated water production. In *World Renewable Energy Congress*, Linkoping, Sweden, 8-13 May. Sweden: Linköping University Electronic Press. DOI: http://dx.doi.org/10.3384/ecp110573881

[15] Zhang H.L., Baeyens J., Degrève J., and Cacères G., 2013. Concentrated solar power plants: Review and design methodology. *Renewable and Sustainable Energy Reviews* 22: 466-481. DOI: https://doi.org/10.1016/j.rser.2013.01.032.

[16] Malan K.J., 2014. *A Heliostat Field Control System.* Master of Engineering Thesis (unpublished). Stellenbosch University, Capetown, South Africa.

[17] Augsburger G., Das A.K., Boschek E., and Clark, M.M., 2016. Thermo-Mechanical and Optical Optimization of the Molten Salt Receiver for a Given Heliostat Field. In *SolarPACES Conference proceedings*. Cape Town, South Africa, 13–16 October 2015. USA: AIP Publishing LLC. DOI: https://doi.org/10.1063/1.4949057.

[18] Wallentinsen B.S., 2016. *Concentrated Solar Power Gas Turbine Hybrid with Thermal Storage*, Master Thesis (unpublished). Norwegian University of Science and Technology, Trondheim, Norway. http://hdl.handle.net/11250/2402290

[19] Hischier I., Hess D., Lipiński W., Modest M., and Steinfeld A., 2009. Heat Transfer Analysis of a Novel Pressurized Air Receiver for Concentrated Solar Power via Combined Cycles. *Journal of Thermal Science and Engineering Applications* 1: 1-6. DOI: https://doi.org/10.1115/1.4001259

[20] Ho C.K., Khalsa S.S., and Siegel N.P., 2009. Modelling on-sun tests of a prototype solid particle receiver for concentrating solar power processes and storage. In *ASME 2009 3rd International Conference on Energy Sustainability*. San Francisco California, USA, 19-23 July. USA: ASME's Publishing. DOI: https://doi.org/10.1115/ES2009-90035

[21] Vogel W., 2010. *Large-scale solar thermal power: technologies, costs, and development*; 2nd ed; Germany: Wiley-VCH.

[22] Augsburger G., 2013. *Thermo-economic optimisation of large solar tower power plants*, Doctoral Thesis (unpublished). École Polytechnique Federale de Laussane, Lausanne: Switzerland. DOI:10.5075/epfl-thesis-5648.

[23] Behar O., Khellaf A., and Mohammedi K., 2013. A review of studies on central receiver solar thermal power plants. *Renewable and Sustainable Energy Reviews* 23: 12–39. DOI: https://doi.org/10.1016/j.rser.2013.02.017.

[24] Ho C.K. and B.D. Iverson. 2014. Review of high temperature central receiver designs for concentrating solar power. *Renewable and Sustainable Energy Reviews* 29: 835-846. DOI: https://doi.org/10.1016/j.rser.2013.08.099

[25] EL Hassani S.E., Ouali H.A.L., Raillani B., Moussaoui M.A., Mezrhab A., and Amraqui S., 2020. Thermal Performance of Solar Tower Using Air as Heat Transfer Fluid under MENA Region Climate. In *5th International Conference on Renewable Energies for Developing Countries (REDEC)*, Marrakech, Morocco, 29-30 June. USA: IEEE Publishing. DOI: 10.1109/REDEC49234.2020.9163893.

[26] Buck R., Bra¨uning T., Denk T., Pfander M., Schwarzbozl, P., and Tellez F., 2002. Solar-hybrid gas turbine-based power tower systems (REFOS). *Journal of Solar Energy Engineering* 124: 2–9. DOI: https://doi.org/10.1115/1.1445444

[27] Heller P., Pfänder M., Denk T., Tellez F., Valverde A., Fernandez J., and Ring A., 2006. Test and evaluation of a solar powered gas turbine system. *Solar Energy* 80: 1225 –1230. DOI: https://doi.org/10.1016/j.solener.2005.04.020

[28] Garcia P., Ferriere A., Flamant G., Costerg P., Soler R., and Gagnepain B., 2008. Solar field efficiency and electricity generation estimations for a hybrid solar gas turbine project in France. *Journal of Solar Energy* 82: 189–197. DOI: https://doi.org/10.1115/1.2807211.

[29] Jabbar M.Q., 2014. Improvement of performance operation and cycle efficiency of Al Anbar combined power plant. In *FPEPM 2014: Annual Conference of the Faculty of Power Engineering and Power Machines*, Sozopol, Bulgaria, 14-17 September. Austria: International Nuclear Information System. https://inis.iaea.org/collection/NCLCollectionStore/Public/47/017/47017656.pdf?r=1.

[30] Camporeale S., Pantaleo A., Ciliberti P., and Fortunato B., 2015. Cycle configuration analysis

and techno-economic sensitivity of biomass externally fired gas turbine with bottoming ORC. *Energy Conversion and Management* 105: 1239–1250. DOI: https://doi.org/10.1016/j.enconman.2015.08.069

[31] Saghafifar M. and M. Gadalla. 2016. Thermo-economic analysis of conventional combined cycle hybridization: United Arab Emirates case study. *Energy Conversion and Management* 111: 358–74. DOI: http://dx.doi.org/10.1016/j.enconman.2015.12.016

[32] Mondal P. and S. Ghosh. 2016. Externally fired biomass gasification-based combined cycle plant: exergo-economic analysis. *International Journal of Exergy* 20: 496-516. DOI: 10.1504/IJEX.2016.078097.

[33] Mondal P. and S. Ghosh. 2017. Exergo-economic analysis of a 1-MW biomass-based combined cycle plant with externally fired gas turbine cycle and supercritical organic Rankine cycle. *Clean Technologies and Environmental Policy volume* 19: 1475–1486. DOI: https://doi.org/10.1007/s10098-017-1344-y

[34] Pantaleo A.M., Camporeale S.M., Sorrentino A., Miliozzi A., Shah N., and Markides C.N. 2017. Solar/biomass hybrid cycles with thermal storage and bottoming ORC: System integration and economic analysis. *Energy Procedia* 129: 724-731. DOI: https://doi.org/10.1016/j.egypro.2017.09.105

[35] Pantaleo A.M., Camporeale S.M., Sorrentino A., Miliozzi A., Shah N., and Markides C.N., 2020. Hybrid solar-biomass combined Brayton/organic Rankine-cycle plants integrated with thermal storage: Techno-economic feasibility in selected Mediterranean areas. *Renewable Energy* 147: 2913–293. DOI: https://doi.org/10.1016/j.renene.2018.08.022.

[36] Morrone P., Algieri A., and Castiglione T., 2019. Hybridisation of biomass and concentrated solar power systems in transcritical organic Rankine cycles: A micro combined heat and power application. *Energy Conversion Management* 180: 757-768. DOI: https://doi.org/10.1016/j.enconman.2018.11.029

[37] Chattopadhyay S. and S. Ghosh. 2020. Thermo-economic assessment of a hybrid tri-generation system making simultaneous use of biomass and solar energy. *Journal of the Brazilian Society of Mechanical Sciences and Engineering* 42: 1-18. DOI: https://doi.org/10.1007/s40430-020-02641-7

[38] Khanmohammadi S., Atashkari K., and Kouhikamali R., 2015. Exergoeconomic multi-objective optimization of an externally fired gas turbine integrated with a biomass gasifier. *Applied Thermal Engineering* 91: 848-859. DOI: https://doi.org/10.1016/j.applthermaleng.2015.08.080

[39] Liu Q., Bai Z., Wang X., Lei J., and Jin H., 2016. Investigation of thermodynamic performances for two solar-biomass hybrid combined cycle power generation systems. *Energy Conversion Management* 122: 252–262. DOI: https://doi.org/10.1016/j.enconman.2016.05.080

[40] Manente G., 2016. High performance integrated solar combined cycles with minimum modifications to the combined cycle power plant design. *Energy Conversion and Management* 111: 186-197. DOI: http://dx.doi.org/10.1016/j.enconman.2015.12.079

[41] Buck R., Giuliano S., and Uhlig R., 2017. Central tower systems using the Brayton cycle. *Advances in Concentrating Solar Thermal Research and Technology, (Elsevier, Amsterdam, 2017)*: 353–382. DOI: http://dx.doi.org/10.1016/B978-0-08-100516-3.00016-2

[42] Ayeleso A.O. and A.K. Raji. 2021. an enhanced solar hybrid Brayton and Rankine cycles with integrated magnetohydrodynamic conversion system for electrical power generation. *International Journal of Renewable Energy Development* 10: 755-767. DOI: https://doi.org/10.14710/ijred.2021.34927

[43] Altafini C.R., Wander P.R., and Barreto R.M., 2003. Prediction of the working parameters of a wood waste gasifier through an equilibrium model. *Energy Conversion and Management* 44: 2763–3277. DOI: https://doi.org/10.1016/S0196-8904(03)00025-6

[44] Fortunato B., Brunetti G., Camporeale S.M., Torresi M., and Fornarelli F., 2017. Thermodynamic model of a downdraft gasifier. *Energy Conversion and Management* 140: 281–294. DOI: http://dx.doi.org/10.1016/j.enconman.2017.02.061

[45] Fortunato B., Camporeale S.M., Torresi M., Fornarelli F., Brunetti G., and Pantaleo A.M., 2016. A Combined power plant fuelled by syngas produced in a downdraft gasifier. In *ASME Turbo Expo* 2016: *Turbomachinery Technical Conference and Exposition*. Seoul, South Korea, 13-17 June 2016. USA: ASME's Publishing LLC. DOI: 10.1115/GT2016-58159

[46] Soltani S., Mahmoudi S.M.S., Yari M., and Rosen M.A., 2013. Thermodynamic analyses of an externally fired gas turbine combined cycle integrated with a biomass gasification plant. *Energy Conversion and Management* 70: 107-115. DOI: https://doi.org/10.1016/j.enconman.2013.03.002

[47] Landau L., Moran M.J., Shapiro H.N., Boettner D.D., and Bailey M., 2018. *Fundamentals of Engineering Thermodynamics*. 9th ed. USA: John Wiley & Sons, New York.

[48] Datta A., Ganguly R., and Sarkar L., 2010. Energy and exergy analyses of an externally fired gas turbine (EFGT) cycle integrated with biomass gasifier for distributed power generation. *Energy* 35: 341–50. DOI: https://doi.org/10.1016/j.energy.2009.09.031.

[49] Gholamian E., Mahmoudi S.M.S., and Zare V., 2016. Proposal, exergy analysis and optimization of a new biomass-based cogeneration system. *Applied Thermal Engineering* 93: 223-235. DOI:

https://doi.org/10.1016/j.applthermaleng.2015.09.095 .

[50] Oyedepo S.O., Fagbenle R.O., and Adefila S.S., 2017. Modelling and assessment of effect of operation parameters on gas turbine power plant performance using first and second laws of thermodynamics. *American Journal of Engineering and Applied Sciences* 10: 412–430. DOI: https://doi.org/10.3844/ajeassp.2017.412.430.

[51] Rahman M.M., Ibrahim T.K., Kadirgama K., Mamat R., and Bakar R.A., 2011. Influence of operation conditions and ambient temperature on performance of gas turbine power plant. *Advanced Materials Research* 189-193: 3007–3013. DOI: https://doi.org/10.4028/www.scientific.net/AMR.189-193.3007

[52] Kayabasßı E., Furtun F., and Özkaymak M., 2017. Investigation of Heat Recovery and Saving Potential of Hot Stoves in Blast Furnaces Investigation of Heat Recovery and Saving Potential of Hot Stoves in Blast Furnaces. In *3rd Iron and Steel Symposium (UDCS'17)*. Karabük, Turkey, 3-5 April 2017. Turkey: Karabük University.

[53] Kadhim H.J., Kadhim T.J., and Alhwayzee M.H., 2019. A Comparative Study of Performance of Al-Khairat Gas Turbine Power Plant for Different Types of Fuel. *IOP Conference Series: Materials Science and Engineering, Volume 671, 3rd International Conference on Engineering Sciences.* Kerbala, Iraq, 4-6 November 2019. IOP Publishing Ltd. DOI: https://doi.org/10.1088/1757-899X/671/1/012015.

[54] Moran M. and H. Shapiro. 2010. *Fundamentals of Engineering Thermodynamics*. 6th ed. India: Wiley Pvt. Limited.

[55] Kiameh P., 2002. *Power Generation Handbook: Selection, Applications, Operation, and Maintenance*. 1st ed. New York: McGraw-Hill.

[56] Tchanche B.F., Loonis P., Petrissans M., and Ramenah H., 2013. Organic Rankine cycle systems Principles, opportunities, and challenges. In *Microelectronics (ICM), 25th International Conference on Microelectronics*. Beirut, Lebanon, 15-18 December. USA: IEEE Publishing LLC. DOI: 10.1109/icm.2013.6735014

[57] Nurhilal O., Mulyana C., Suhendi N., and Sapdiana D., 2016. The simulation of organic Rankine cycle power plant with n-pentane working fluid. In *AIP Conference Proceedings* 1712. Jatinangor, Indonesia, 2–3 September 2015. USA: AIP Publishing LLC. DOI: https://doi.org/10.1063/1.4941880.

[58] Rajesh R. and P.S. Kishore. 2018. Thermal Efficiency of Combined Cycle Power Plant. *International Journal of Engineering and Management* 8: 229–234. DOI: https://doi.org/10.31033/ijemr.8.3.30

[59] Petrakopoulou F., Sánchez-Delgado S., Marugán-Cruz C., and Santana D., 2017. Improving the efficiency of gas turbine systems with volumetric solar receivers. *Energy Conversion and Management* 149: 579–592. DOI: https://doi.org/10.1016/j.enconman.2017.07.058

[60] European Commission, Directorate-General for Research and Innovation., 2005. *SOLGATE, solar hybrid gas turbine electric power system*. Luxembourg: Office for official publications of the European communities. ISBN 92-894-4592-0.

[61] Aldali Y. and K. Morad. 2016. Numerical simulation of the integrated solar/North Benghazi combined power plant. *Applied Thermal Engineering* 108: 785-792. DOI: https://doi.org/10.1016/j.applthermaleng.2016.07.178

[62] Ahmad A.D., Abubaker A.M., Najjar Y.S.H., and Manaserh Y.M.A., 2020. Power boosting of a combined cycle power plant in Jordan: An integration of hybrid inlet cooling and solar systems. *Energy Conversion and Management* 214: 112894 (1-14). DOI: https://doi.org/10.1016/j.enconman.2020.112894.